 DOI: 10.1002/masy.201050532

Magnetically Induced Heating in Elastomeric Nanocomposites - Theory and Experiment

Igal Levine,[1] *Regev Ben Zvi,*[1] *Moritz Winkler,*[2] *Annette M. Schmidt,*[2] *Moshe Gottlieb**[1]

Summary: Magnetic nanoparticles are known to generate heat when exposed to an alternating external magnetic field. A multi-scale model for the heat generation by magnetic nanoparticles embedded in an elastomeric material has been developed. The model affords the determination of the unsteady-state temperature profiles in the particles and in the surrounding polymeric medium by numerically solving the Equation of energy. We obtained the complete thermal history of the system as a function of all relevant parameters including particle size, particle volume fraction, thermal properties of the particle and the medium, and details of the imposed magnetic field. The predicted results are in good agreement with experimental data obtained on liquid crystalline elastomers.

Keywords: elastomers; magnetic nanoparticles; magnetically induced heating; magnetoactive polymers; nanocomposites

Introduction

Magnetic nanoparticles (MNP) embedded in a polymeric matrix are known to generate heat when exposed to an alternating external magnetic field.[1] It has been recently demonstrated that these thermal effects may be used to obtain magnetoactive polymers and elastomers.[2] Two separate mechanisms are responsible for the generation of magnetically induced heating: the viscous heating in the surrounding fluid as a result of the flow generated by the particle motion, and the Néel relaxation of the internal magnetic moment.[3] In the case of polymers below their glass transition temperature or for elastomers, only the latter is relevant. Yet, even for polymer melts or low viscosity fluids, there is a critical particle size which depends on the magnetic properties of the particle, below which the Néel mechanism dominates. In order to achieve a better understanding of the response of magnetoactive polymeric systems in general, and elastomers, in particular (systems in which Néel relaxation is clearly dominating), a detailed theoretical analysis of the thermal effects is warranted. Such an analysis will also enable the judicious design of magnetoactive elastomers. Some studies carried out in the past have modeled the system by approximating it to a single particle embedded in an infinite medium[4–8] and neglecting the internal temperature gradient within the magnetic particle.[5–7] Alternatively, the particles and the matrix have been replaced by an isotropic ''effective medium'' of homogeneous properties surrounded by an infinite liquid.[7–9] In other cases, the thermal behavior has only been analyzed in terms of the global heat generation and the average temperature disregarding internal temperature gradients.[9] While some of these approximations may be appropriate under certain conditions, no detailed justification has been previously provided. In this paper we

[1] Chemical Engineering Department and Ilse Katz Institute for Nanoscale Science and Technology, Ben Gurion University of the Negev, Beer Sheva 84105, Israel
E-mail: mosheg@cs.bgu.ac.il
[2] Institut für Organische Chemie und Makromolekulare Chemie, Heinrich-Heine-Universität Düsseldorf, D-40225 Düsseldorf, Germany

Copyright © 2010 WILEY-VCH Verlag GmbH & Co. KGaA, Weinheim

describe a multi-scale model dealing with a finite-size system (as opposed to the infinite systems used above) and taking into account the temperature within the particles as well as in the polymeric matrix surrounding them. The predictions of the model are compared to experimental data obtained for a magnetically actuated elastomer.[10,11] Due to the experimental difficulties in measuring nano- and micro-scale thermal effects, only macro-scale effects are available for comparison with the theoretical results.

Theoretical Models

Let us consider a collection of monodisperse spherical MNPs of radius R_1, homogeneously distributed in a polymer matrix. Influenced by the experimental setup used for model validation,[10,11] we assume the polymer composite sample is cylindrical in shape and initially in thermal equilibrium with the surroundings, i.e. its temperature is uniform and identical to the temperature of the surrounding air. Upon imposition of an external alternating magnetic field, particle rotation and motion is suppressed such that only Néel heating is of any consequence. We further assume that the physical, magnetic, and heat generating properties of the particles and the properties of the polymer matrix are all independent of temperature. It is also assumed that the polymer matrix does not undergo any phase transitions or other non-thermal thermodynamic processes, i.e. any energy generated by the particles is used up entirely to heat the particles and the polymer or is lost to the surroundings. The magnetic interaction between neighboring particles is neglected. This latter assumption is easily justified by inspecting the ratio of the magnetic dipolar energy to the thermal energy: $[m^2/\mu_0(2L)^3]/k_BT$, where $m = \mu_0 V_M \chi H$ is the magnetic moment of the MNP, μ_0 is the permeability of free space, V_M is the volume of the magnetic core, χ is the susceptibility, H the applied magnetic field, L is half the center-to-center separation distance between two adjacent MNPs, T is the absolute temperature, and k_B is the Boltzmann constant. For a typical experimental system containing magnetite particles with volume fractions not exceeding 0.02, this ratio is below 0.01, hence the magnetic interaction between neighboring MNPs can be ignored. Finally, we also neglect any contribution of convective or irradiative heat transport.

Nanoscale: Single Particle Model (short times)

Upon application of the external high frequency alternating magnetic field, the temperature in the MNPs will start to rise, leading to the creation of a temperature gradient inside the particle. Gradually, the polymer matrix in the vicinity of the particles will heat up as well. Due to the large difference in thermal conductivities of the MNP and polymer matrix it is expected that most of the temperature gradient will be found in the polymer and the temperature differences within the particle will diminish. Eventually, at some time t' the temperature between adjacent particles at the same radial distance from the sample center will become relatively uniform and heat transfer processes between the sample and its surroundings rather than interparticle processes assume the leading role. At this initial nanometric time scale, the focus is on individual MNPs at sufficiently short times such that heat removal to the surroundings of the entire macroscopic sample may be neglected.

For a spherically symmetric particle, the Equation of energy in spherical coordinates is:[12]

$$\rho\hat{C}_p\frac{\partial T}{\partial t} = k\frac{1}{r^2}\frac{\partial}{\partial r}\left(r^2\frac{\partial T}{\partial r}\right) + P' \qquad P' = \begin{cases} P & 0 \le r \le R_1 \\ 0 & R_1 < r \le L \end{cases} \tag{1}$$

where ρ is the density, $\hat{C}_p$ the heat capacity, k the coefficient of thermal conductivity, and R_1 and L are as defined above. The rate of internal heat generation in the MNP *per unit volume of magnetic core*, P, is assumed to be constant and temperature independent.

Copyright © 2010 WILEY-VCH Verlag GmbH & Co. KGaA, Weinheim

Equation (1) is solved for each one of the two systems (particle and polymer) with their corresponding values for the physical properties and with the following initial (*I.C.*) and boundary (*B.C.*) conditions:

$$I.C. \quad T_{1,2}(r,0) = T_0$$
$$B.C.1 \quad \text{at} \quad r = 0, \frac{\partial T_1}{\partial r} = 0$$
$$B.C.3 \quad \text{at} \quad r = R_1, k_1 \frac{\partial T_1}{\partial r} = k_2 \frac{\partial T_2}{\partial r}$$
$$B.C.2 \quad \text{at} \quad r = \mathrm{R}_1, T_1 = T_2$$
$$B.C.4 \quad \text{at} \quad r = L, \frac{\partial T_2}{\partial r} = 0$$

Indices 1 and 2 represent the particle and the polymer respectively. *B.C.* 1 and *B.C.* 4 result from symmetry considerations; the latter, however, is valid only for sufficiently short times when all the heat generated is accumulated within the sample and heat removal to the external surroundings can be neglected.

It is useful to analyze the systems in terms of the local (particle) Biot number (Bi_p)[13] which represents the ratio of the internal resistance to heat transfer in the MNP to the external resistance in the polymer matrix: $Bi_p = \frac{k_2}{k_1} \cdot \frac{1}{1-\xi}$ where the dimensionless particle radius $\xi = R_1/L$ is directly related to the MNP volume fraction φ and organization (e.g. $\xi = 1.14\ \varphi^{1/3}$ for body-centered cubic structure and $1.24\ \varphi^{1/3}$ for simple cubic).

Microscale: Cylindrical Shells Model

At intermediate times ($t' < t < t''$, where t' has been defined above as the time by which the temperature between particles at the same radial distance from the axis of symmetry of the cylindrical sample will become uniform, and t'' is the time when temperature variations within the entire sample become negligible) we consider the cylindrical sample as a collection of concentric cylindrical shells. Each such shell is assumed to be composed of an "effective-material" with uniform distribution of heat sources (MNPs) and system-averaged thermal properties. We ignore end effects assuming the heat loss through the two flat surfaces of the cylinder is negligible relative to the heat lost through the cylindrical surface (i.e. cylinder length is much larger than its diameter). Although our choice of geometry is dictated by the experimental sample,[10,11] the model could be easily adjusted to other geometries. The energy balance in each shell, can be described by the Equation of energy in cylindrical coordinates: [12]

$$\tilde{\rho}\overline{C}_p \frac{\partial T}{\partial t} = \tilde{k}\frac{1}{r}\frac{\partial}{\partial r}(r\frac{\partial T}{\partial r}) + S_M \tag{2}$$

The tilde indicates volume averaged properties and the overbar indicates mass averaged properties. The rate of heat generation *per unit volume of composite sample* S_M is $S_M = P \cdot \varphi$, assuming the MNP volume fraction φ is uniform and identical for all shells and P is temperature independent.Equation (2) is solved with the following *I.C.*s and *B.C.*s:

$$I.C.1 \quad T(r,0) = T_a$$
$$I.C.2 \quad T(r,\infty) = T_{\max}(r)$$
$$B.C.1 \quad \text{at} \quad r = 0, \frac{\partial T}{\partial r} = 0$$
$$B.C.2 \quad \text{at} \quad r = \mathrm{R}, q_r = h(T_R - T_a)$$

where $T_{\max}$ is the equilibrium temperature, T_R the surface temperature, $q_r$the radial diffusive heat flux, T_a is the surrounding air temperature, h is the convective heat transfer coefficient of the surrounding air, and R the cylindrical sample radius. Note that although we use *I.C.* 1, the solution obtained for Equation (2) is valid only for times $t > t'$ and t' is determined from the solution of the nanoscale model (Equation 1).Solving analytically Equation (2) at long times (equilibrium, $t \to \infty$) yields:

$$T_{\max} - T_a = \frac{P\varphi}{h}\left\{\frac{hR^2}{4[k_1\varphi + k_2(1-\varphi)]}\left[1 - \left(\frac{r}{R}\right)^2\right] + \frac{R}{2}\right\} \tag{3}$$

The equilibrium temperature rise averaged over the entire cylindrical sample is:

$$\langle T_{\max} - T_a \rangle = \frac{P\varphi R}{2h}\left(\frac{Bi_s}{2} + 1\right) \tag{4}$$

where Bi_s is the global Biot number (as opposed to Bi_p, the particle Biot number

Copyright © 2010 WILEY-VCH Verlag GmbH & Co. KGaA, Weinheim

defined above) which represents the ratio of the resistance to heat transfer inside the sample to the external resistance to heat transfer in the surrounding air:

$$Bi_s = \frac{h}{\tilde{k}}\left(\frac{V}{A}\right) = \frac{hR}{2[k_1\varphi + k_2(1-\varphi)]} \quad (5)$$

V and A are the volume and surface area of the cylindrical sample, respectively.

Macroscale: Lumped Model

It is possible that under certain conditions and after some time has elapsed ($t > t''$), the temperature gradients within the sample become vanishingly small and we may consider only the time dependent average temperature change ignoring spatial variation in temperature. For this to occur will depend on the relative rates of heat generation, heat conduction in the polymer and heat removal to the surroundings but it is usually justified if $\mathrm{Bi_s} << 1$.[13] In such a case, the entire sample may be considered as a continuous ''effective medium'' with volume-averaged thermal properties and uniform temperature throughout. Thus, the sample temperature is approximated by the time dependent volume average temperature:

$$\langle T(t)\rangle = \frac{1}{V}\int_V TdV \quad (6)$$

The Equation of energy in terms of $\underline{q}$, the conductive heat flux in the system:

$$\rho\hat{C}_p\frac{\partial T}{\partial t} = -\nabla\cdot + S_M \quad (7)$$

can easily be solved analytically with the following I.C. and B.C.:

$$\begin{aligned} &I.C.1 \quad \text{at } t = 0, \langle T\rangle = T_a \\ &I.C.2 \quad \text{at} t \to \infty, \langle T\rangle = \langle T\rangle_{\max} \\ &B.C.1 \quad \text{at } r = \mathrm{R}, q_r(t) = h(\langle T(t)\rangle - T_a) \end{aligned}$$

Integrating (7) over the entire volume we may obtain:

$$\begin{aligned} \rho\hat{C}_p\frac{d}{dt}\int_V TdV &= -\int_A \underline{n}\cdot\underline{q}dA + S_M V \\ \rho\hat{C}_p V\frac{d\langle T\rangle}{dt} &= -hA(\langle T\rangle - T_a) + S_M V \end{aligned} \quad (8)$$

At very long time the system will eventually reach equilibrium, $\frac{d\langle T\rangle}{dt} = 0$:

$$S_M V = qA = hA(\langle T\rangle_{\max} - T_a) \quad (9)$$

We define a relative temperature $\theta = (\langle T\rangle - T_a)$ and a system time constant $\tau = \rho\hat{C}_p V/hA$. Rearranging Equation (8) we obtain $d\theta/dt = -\theta/\tau + S_M\big/\rho\hat{C}_p$ and solving

$$\theta = \frac{S_M}{\rho\hat{C}_p}\tau\left(1 - e^{-t/\tau}\right) \quad (10)$$

Given a set of experimental data, the value of S_M (and P) is extracted from $(d\theta/dt)_{t=0} = S_M\big/\rho\hat{C}_p$ or from the measured $\langle T\rangle_{\max}$ and Equation (9). The value of τ or h can be obtained from Equation (10).

Experimental Part

Experimental data on the magnetic heating of an elastomeric nanocomposite have been obtained on a system composed of a side chain liquid-crystal elastomer (LCE) loaded with MNPs. Only the most relevant experimental details concerning the synthesis, preparation, and magnetic heating are outlined here, whereas a complete description is available elsewhere.[10,11] The elastomers consisted of a polysiloxane backbone with 4-(3-butenoxy)benzoic acid 4-metoxy-phenyl ester type LC-side groups. Magnetite (Fe_3O_4) particles with a core diameter of 12 nm were prepared by alkaline hydrolysis of ferrous and ferric chloride, followed by stabilization of the precipitated particles in toluene with *N*-oleoylsarcosine. LCEs with particle content up to 1.8 vol.-% were obtained. The homogeneity of the particle dispersion in the polymer matrix was verified by TEM.[11]

Magnetic heating experiments were performed on a Huettinger High Frequency Generator TIG 5.0/300 with a copper inductor ($l = 50$ mm, $d_\mathrm{I} = 35$ mm, $n = 5$). The apparatus was operated at 300 kHz at a maximum induction power of 5.0 kW and maximum amplitude field

Copyright © 2010 WILEY-VCH Verlag GmbH & Co. KGaA, Weinheim

strength of 42.6 $kA \cdot m^{-1}$. MNP loaded LCE samples were prepared in a cylindrical vial with a diameter of 3 mm and a height of 10 mm which was placed in the center of the induction coil. The temperature was recorded with an Opsens OTG-A fiber optic system.[10,11]

Results and Discussion

From the lumped model (Equation 10) using 5 sets of data obtained at different MNP contents, the average value of h was determined to be 20 $W\,m^{-2}\,K^{-1}$. The same data was used to determine the average experimental value of P to be 1.6×10^8 W m^{-3}. These values are employed throughout. It should be noted that, in principle, it is possible to calculate P using the result obtained by Rosensweig,[9] rather than extracting it from experimental data, but that requires precise values of the magnetic properties of the MNPs which are not available to us at the necessary accuracy. The use of Equation (10) resulting from the "lumped" model is justified by the estimated global Biot number ($\sim$0.1).

The calculation is carried out for two different local Biot numbers $Bi_p = 0.03$ (Figure 1a) and $Bi_p = 1.00$ (Figure 1b) obtained by changing the value of the thermal conductivity coefficient of the polymer while keeping all other values unchanged. Due to the relatively small resistance to heat transfer inside the particle in the former case (small Bi_p), most of the temperature gradient is found in the surrounding polymer, and the particle temperature is nearly uniform. In contrast, if we select a matrix with a 30 times higher thermal conductivity, a considerable temperature gradient is observed inside the MNP at short times as is clearly observed in Figure 1b. Solution such as that depicted in Figure 1 allows the determination of t', the time by which the temperature between two neighboring particles is practically uniform. For the magnetite-PDMS LCE systems examined here, we find this to occur at $F_0 = 10^5$ or $t' \approx 1\,\mu s$, and for the higher Biot system at $F_0 = 10^3$ ($t' \approx 10$ ns).

Figure 2a illustrates the effect of the rate of heat generation P on the temperature profile by comparing the temperature profiles for different P values at identical time. As expected, increasing/decreasing P results in a directly proportional increase/decrease in MNP temperature. A similar, yet smaller, effect is observed in the midpoint ($r/L = 1$) polymer temperature. In Figure 2b, the effect of the thermal conductivity of the polymer matrix is examined. As the thermal conductivity of the polymer is increased, heat is more readily transported into the polymer, resulting in a lower temperature at the

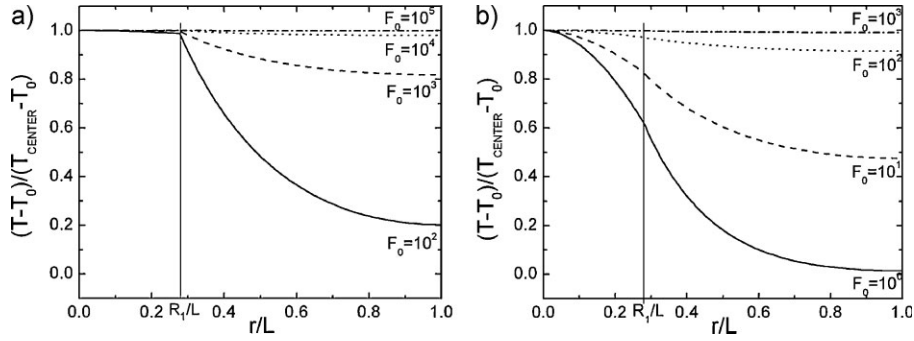

Figure 1.
Evolution of the temperature profiles with time for magnetite particles at two different polymeric matrices. The different curves represent different values of elapsed dimensionless time $F_0 = \alpha_1 \cdot t/R_1^2$. (a) $k_2 = 0.15$ W m^{-1} K^{-1}, $Bi_p = 0.03$; (b) $k_2 = 5.06$ W m^{-1} K^{-1}, $Bi_p = 1.00$. Magnetite properties: $R_1 = 6$ nm, $\varphi = 0.0145$, $P = 1.6 \times 10^8$ W m^{-3}, $k_1 = 7$ W m^{-1} K^{-1}, $\hat{C}_{p,1} = 608$ J kg^{-1} K^{-1}, $\rho_1 = 5170$ kg m^{-3}. Polymer matrix properties: $\hat{C}_{p,2} = 2200$ J kg^{-1} K^{-1}, $\rho_2 = 1000$ kg m^{-3}. The vertical line indicates the particle surface.

Copyright © 2010 WILEY-VCH Verlag GmbH & Co. KGaA, Weinheim

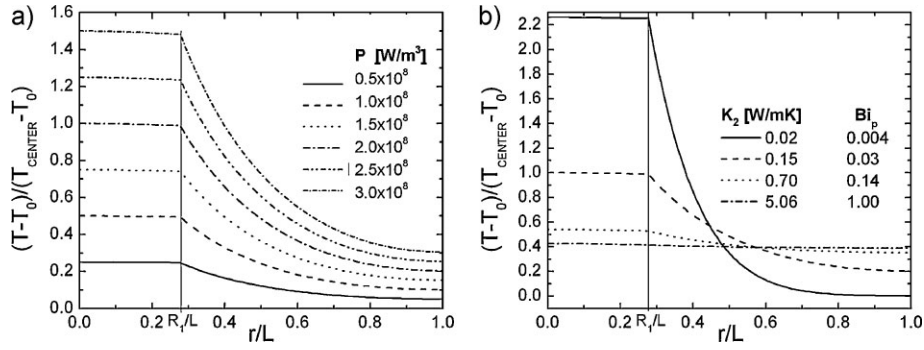

Figure 2.

Effect of system parameters on the temperature profiles for $F_0 = 100$ and $\varphi = 0.0145$. (a) Effect of the heat production rate, P, with $P = 2 \times 10^8$ W m^{-3} taken as reference and all other parameter values identical to those in Figure 1a. (b) Effect of the thermal conductivity of the polymer, k_2, with $k_2 = 0.15$ W m^{-1} K^{-1} taken as reference and all other parameter values identical to those in Figure 1a. The horizontal line indicates the position of the particle edge.

magnetic core and a more even distribution of heat throughout the system. In contrast, low thermal conductivity of the polymer effectively insulates the particle, resulting in high core temperatures with little heating of the polymer. Thus, for the preparation of effective magneto-responsive composites, attention should be paid to the thermal conductivity of the polymer or rather, the Bi_p value, although in most cases these times are extremely short.

Now, that it has been established that after the very short time of the order of few μs, only a radial dependence of the temperature in the composite should be considered, we may confidently apply the Cylindrical Shell model. Equation (2) with the associated *I.C.* and *B.C.* is solved numerically. In Figure 3, the calculated value of the temperature (relative to the ambient air temperature) at the center of the cylindrical sample is shown as function of time for four different MNP concentrations and in comparison with experimental data on systems with similar properties. As clearly seen in these figures, the calculated results are in good agreement with the experiments, with deviations smaller than 15%.

Equation (3) allows determination of the radial temperature distribution after the system has been equilibrated with its surroundings. The calculated values are depicted in Figure 4 showing a relatively flat temperature profile with temperature differences between the center and the sample edge of less than 5 K. This result is consistent with the small Bi_s values (0.06–0.08) in the experimental systems.

The center-line equilibrium temperature obtained from the Cylindrical Shells model (Equation 3) is compared to the value predicted by the Lumped model and to the experimental data in Figure 5. The difference between the values predicted by the two models are negligibly small, which is not surprising in view of the low Bi_s values for the experimental systems used here. Good agreement is obtained with the experimental data. The observed deviations may be attributed to a temperature dependence of the physical properties and the heating power, and the distribution in particle size. In addition, nematic-isotropic phase transitions, known to occur in these LCE systems[10,11] which are expected to impact the heat balance as well as the values of the physical properties, have also been ignored. These effects will be further examined in future work.

Finally, we use Equation (3) to estimate the potential for temperature rise in cylindrical samples with different diameters. The time to reach equilibrium is also easily determined ($t_{eq} = 5\,\tau$). As can be seen in Figure 6, substantial heating may be

Copyright © 2010 WILEY-VCH Verlag GmbH & Co. KGaA, Weinheim

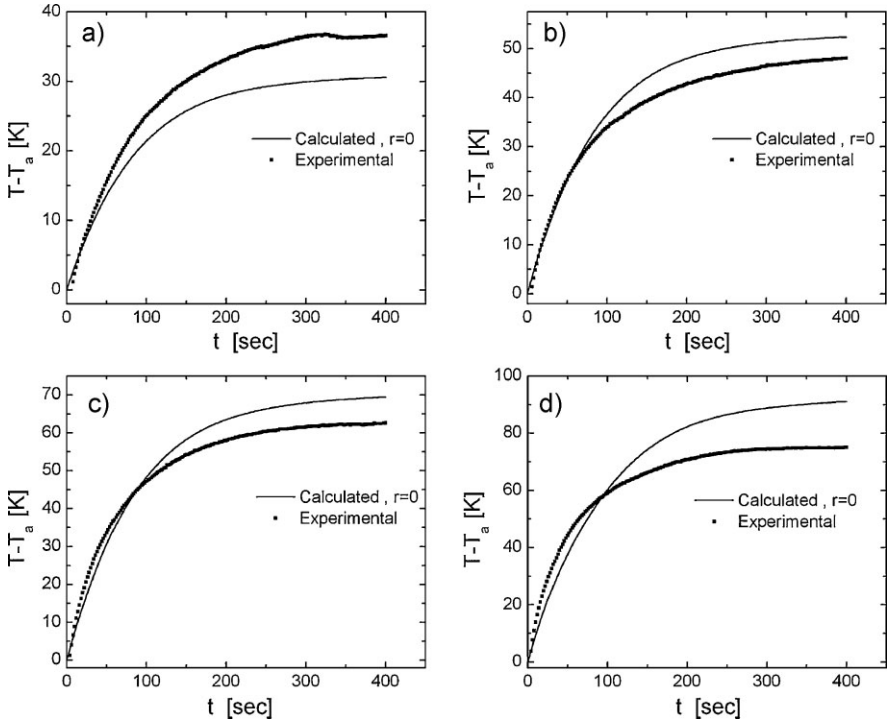

Figure 3.
Temperature rise of samples with varying MNP concentration: (a) 0.48%; (b) 0.83%; (c) 1.10%; (d) 1.45%. Calculated data were obtained from the solution of the Cylindrical Shell model.

achieved, depending on the sample size. These results should be considered with care since temperature dependence of properties and especially P, are probably important considering the predicted temperature range. In addition, these values are in excess of the Curie temperature of magnetite ($T_{\text{Curie}} \sim 575\,^{\circ}\text{C}$). Despite the

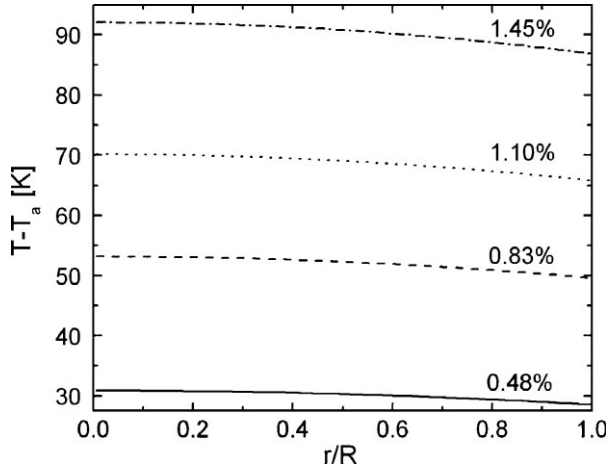

Figure 4.
Calculated equilibrium temperature profile for the Cylindrical Shells model.

Copyright © 2010 WILEY-VCH Verlag GmbH & Co. KGaA, Weinheim

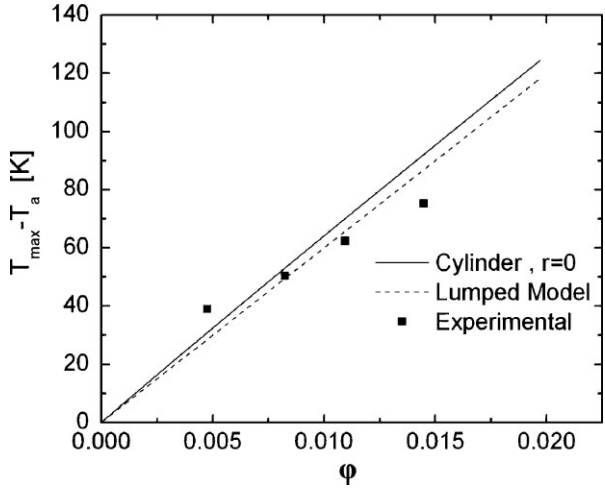

Figure 5.
Comparison between the models at equilibrium

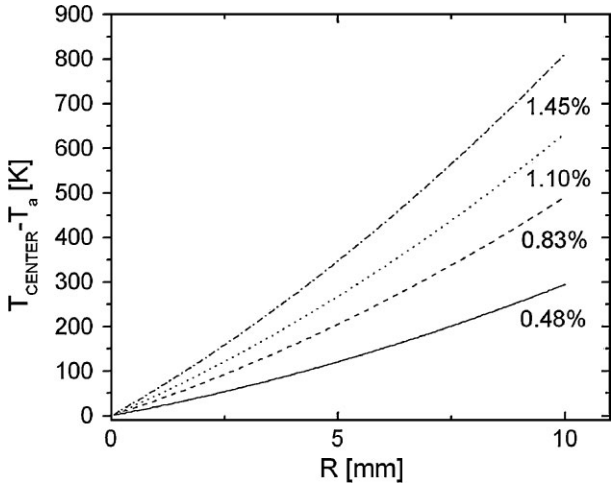

Figure 6.
Effect of sample size on center-line equilibrium temperature. Calculation by Cylindrical Shells model.

above, Figure 6 serves to point out the usefulness of the models developed here as a tool for the design of magneto-responsive composite systems.

Conclusion

The multi-scale model developed to describe the magnetic heating of a nano-composite has been successfully applied to the analysis of the thermal history of a magnetite-LCE system. It was found that in this system the temperature between individual nanoparticles at the same radial position becomes uniform after very short times of the order of few microseconds. Thus, micro- and macro-scale models may be used with proper justification.

The calculated results are in good agreement with the experimental results with deviations of 15% or lower, and may be improved by including the temperature dependence of the material properties and

Copyright © 2010 WILEY-VCH Verlag GmbH & Co. KGaA, Weinheim

the particle volumetric heating power and taking into account the nematic-isotropic phase transition.

[1] G. Glöckl, R. Hergt, M. Zeisberger, S. Dutz, S. Nagel, W. Weitschies, *J. Phys.: Condens. Matter* **2006**, *18*, S2935.
[2] A. M. Schmidt, *Macromol. Rapid Commun.* **2006**, *27*, 1168.
[3] M. Feyen, E. Heim, F. Ludwig, A. M. Schmidt, *Chem. Mater.* **2008**, *20*, 2942.
[4] H. S. Carslaw, J. C. Jaeger, "*Conduction of Heat in Solids*", 2nd ed., Oxford University Press, Oxford 1959.
[5] W. L. Nyborg, *Phys. Med. Biol.* **1988**, *33*, 785.
[6] P. Keblinski, D. G. Cahill, A. Bodapati, C. R. Sullivan, T. A. Taton, *J. Appl. Phys.* **2006**, *100*, 054305.
[7] Y. Rabin, *Int. J. Hyperthermia* **2001**, *18*, 194.
[8] W. Andrä, C. G. d'Ambly, R. Hergt, I. Hilger, W. A. Kaiser, *J. Magnetism Magn. Mater.* **1999**, *194*, 197.
[9] R. E. Rosensweig, *J. Magnetism Magn. Mater.* **2002**, *252*, 370.
[10] A. Kaiser, M. Winkler, S. Krause, H. Finkelmann, A. M. Schmidt, *J. Mater. Chem.* **2009**, *19*, 538.
[11] M. Winkler, A. Kaiser, S. Krause, H. Finkelmann, A. M. Schmidt, *Macromol. Symp.* **2010**, this volume.
[12] R. B. Bird, W. E. Stuart, E. N. Lightfoot, "*Transport Phenomena*", 2nd ed., J. Wiley & Sons, New York 2007, p. 335.
[13] F. Kreith, "*Principles of Heat Transfer*", 3rd ed., Harper & Row, New York 1973, p. 140.

Copyright © 2010 WILEY-VCH Verlag GmbH & Co. KGaA, Weinheim